

# The use of microgravity technique in archaeology: A case study from the St. Nicolas Church in Pukanec, Slovakia

Jaroslava PÁNISOVÁ<sup>1</sup>, Roman PAŠTEKA<sup>2</sup>

<sup>1</sup> Geophysical Institute of the Slovak Academy of Sciences  
Dúbravská cesta 9, 845 28 Bratislava, Slovak Republic; e-mail: geofjapa@savba.sk

<sup>2</sup> Department of Applied and Environmental Geophysics, Faculty of Natural Sciences, Comenius University, Mlynská dolina, 842 15 Bratislava, Slovak Republic;  
e-mail: pasteka@fns.uniba.sk

**Abstract:** The detection of subsurface cavities, such as crypts, cellars and tunnels, in churches and castles belongs to successful applications of the employment of surface gravity measurement techniques in archaeo-prospecting. The old historic building exploration requires using of non-invasive methods, and hence the microgravity technique is a proper candidate for this task. On a case study from the Roman-Catholic Church of St. Nicolas in the town Pukanec the results of using microgravity for detection and delineation of local density variations caused by a near-surface void are shown. The acquired negative anomaly in the residual Bouguer anomalies field suggested the presence of a possible void feature. Euler deconvolution and 3D modelling were used to estimate the depth and shape of the anomalous source. Additionally, measurements of the vertical gravity gradient on several stations were performed. We tested how the use of a downward continuation of gravity, utilizing the real vertical gravity gradient, influences the shape and amplitude of the final Bouguer anomaly map.

**Key words:** microgravity, vertical gravity gradient, Bouguer anomaly, archaeo-prospecting, cavity detection, historic buildings

## 1. Introduction

The detection of subsurface cavities using the microgravity technique requires the sensing of localized negative anomalies in a background of regional or large scale variations of gravity. Cavities may be natural, such as solution cavities in limestones; or man-made, such as tunnels, mine workings and crypts. A negative anomaly is not always the case. The buried tomb

can give rise to a positive anomaly in the case that the tomb had collapsed (*Bishop et al., 1997*). Air-filled cavities give the largest negative anomaly amplitude condition because of the complete absence of dense material in the target. In comparison with air voids, water-filled cavities offer a gravity anomaly effect which is only about 60% of the same cavity containing air; a rubble- or mud-filled anomaly is about 40% that of air filled one (*Owen, 1983*). The rock surrounding the man-made cavity is often disturbed and the associated fracturing may extend to two or more diameters away from the cavity. The effective size of cavity is dependent also on its connectivity and the genesis of that cavity in its host rock (*Bishop et al., 1997*). This cavity enhancement is often termed a “halo” effect and ensures that the cavity can be indirectly sensed.

The vertical gradient of gravity can be used for cavity detection because it gives supplementary and more accurate information on the distribution of density inhomogeneities in shallow depths up to about 15 m. *Fajkiewicz (1976)* applied the method of vertical gravity gradient in a variety of mining and engineering problems in Poland, particularly in connection with the detection of shallow abandoned mine workings. *Butler (1984)* employed microgravity and gradient techniques to the detection and delineation of shallow subsurface cavities and tunnels in Florida.

The non-invasiveness is the main advantage of using microgravity technique in archaeology, but on the other hand this method is very time-consuming. Nowadays, the leader in exploration and assessing of the cultural heritage is the Ground Penetrating Radar (GPR). Successful applications of microgravity technique in historic objects exploration can be found only in a few papers. *Blížkovský (1979)* solved the task of crypt identification under the floor of St. Wenceslas church in Tovačov. A significant minimum obtained from the Bouguer anomaly map was interpreted as being caused by an unknown crypt. This interpretation was proved by excavation work and several tombs were discovered. *Lakshmanan and Montlucon (1987)* proved that microgravity technique is applicable also inside the pyramids. On the basis of their results, the “stores” of sand were discovered near the Queen’s chamber in the Great Pyramid which may be related to new and unknown chambers. In Slovakia, archaeological excavations in the former church of St. Catherine (in Malé Karpaty Mts.) were performed using the combination of microgravity survey with resistivity imaging, and a medieval crypt



Fig. 1. Left – W view of the St. Nicolas church, right – a position of the Pukanec-city, 25 km SW from Banská Štiavnica (southern central Slovakia).

was discovered (*Pašteka and Zahorec, 2000*). Successful application of GPR and microgravity was realized in the St. Nicolas church in Trnava (*Pašteka et al., 2007; Terray and Pašteka, 2007*), where 8 new crypts have been detected and also verified by means of video-inspection. The application of microgravity technique in industrial archaeology is presented in *Cuss and Styles (1999)*.

## 2. The site

The Roman-Catholic Church of St. Nicolas is the most important historical monument of the former mining town of Pukanec located in the southern part of central Slovakia (Fig. 1). The town lies on the base of the southeast slopes of the Štiavnica Mountains, in the northern part of the Bátovská fold. The range is an eroded caldera created by the collapse of an ancient (cenozoic) volcano. There are many old mines due to the richness of ore deposits, located on the hills near towns of Pukanec and Banská Štiavnica. The Church of St. Nicolas is the unique representative of the Gothic architecture in this region. It is known, based on available art-historical sources,

that the church was built in two stages. The nave originated in the fourteenth century after the foundation of the town. In the beginning of the fifteenth century, a new aisle was built to the northern side of the church. From the Reformation till 1940 the nave was separated from the aisle by a single wall. Some explorers claim that the aisle was built on the original Romanesque foundations and originally it had two presbyteries, one of which is now the sacristy. In the year 2003, the historical, structural and restoration research of the Church of St. Nicolas has started. Microgravity survey was employed to investigate the ground below the floor in the nave in order to locate a possible buried chamber, which might be a part of an old tunnel system underlying the town.

### 3. Microgravity and vertical gradient surveys

Microgravity observations were made on a 10 m × 20 m grid with a spacing of 1 m (somewhere less than 1 m due to restrictions on examined area) in two phases in 2008. Local coordinate system was used with the starting point (50, 50) located close to church steps in the western part of the nave (Fig. 2). Globally, 111 points were positioned and measured on a floor in the nave and apse. Each measured station position had been determined with a sufficient accuracy in horizontal and vertical directions. Elevations of measured points have been determined by means of technical levelling with the instrument Fennel Qeo10 in a closed loop (starting from the base station). The loop error was  $\pm 0.001$  m and in the case of such a small error, obtained elevation values have not been adjusted. The map of measured elevations is displayed in Fig. 2. Seven stations with the highest elevations have been positioned on wooden stairs in the area of the apse. Another eleven points have been positioned on a lower wooden stair in the entrance of the apse (Fig. 2, all 18 points on wooden stairs are denoted by a triangle).

Gravity data were collected using the relative gravimeter Scintrex CG-5. The instrument has a quoted standard field repeatability of less than  $5 \mu$  Gal. The corrections of Earth tides, tilts of the measuring system, temperature changes and a long-term drift were implemented automatically during the measuring process. For a correct determination of the short-term drift, the base station readings were recorded every hour during the survey on a selected base station (Fig. 2). Repeated readings on 11 control stations (i.e.,

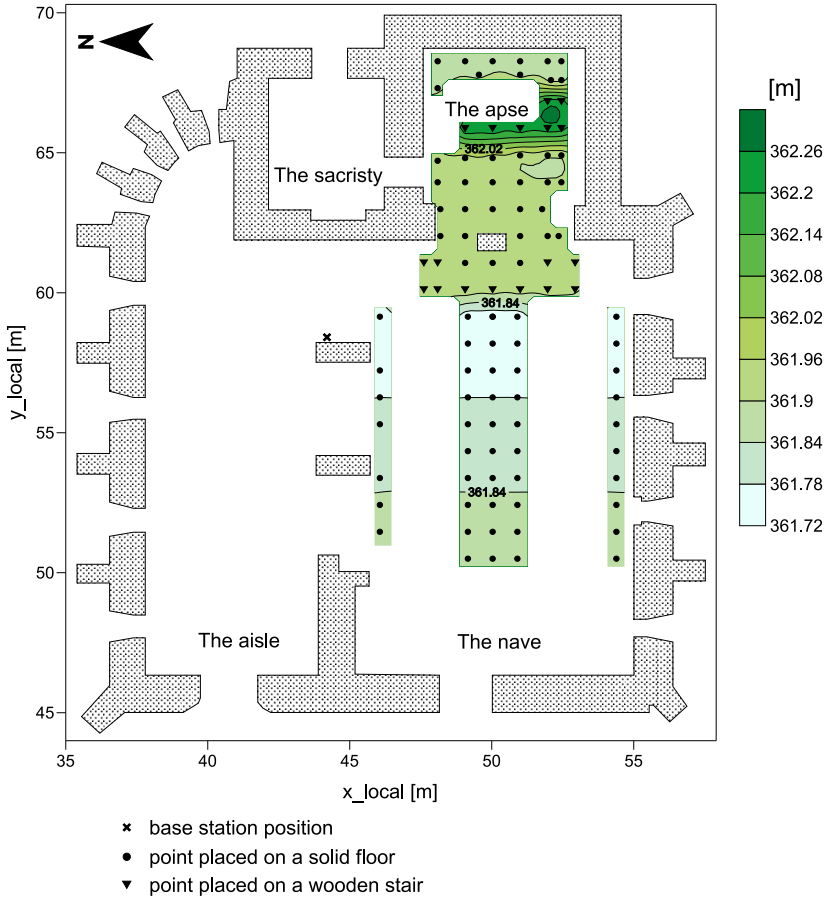


Fig. 2. The map of measured heights in [m] with positions of measured stations and a plan of the church’s walls (represented with dotted areas);  $x_{local} [m]$  and  $y_{local} [m]$  are the horizontal and vertical axes of the used local coordinate system.

10 percent from the total number of points) were taken as a part of the survey, which provided the root-mean-square error of less than  $4 \mu \text{Gal}$ .

In addition to the microgravity survey, the vertical gradient survey was conducted on 3 points ((50, 64), (52, 64) and (52, 66)) in the apse in January 2009. The purpose of the vertical gradient survey was to determine the real vertical gravity gradient and use it for the downward continuation of seven stations with the highest elevations. From the point of the interpretation,

it is better when all measuring points have approximately identical elevation. These seven stations, denoted in Fig. 2 by a triangle, are located on wooden steps in the apse with the average elevation difference of 0.33 m. The idea of the downward continuation of gravity on these stations comes from the fact that the wooden steps are empty, so the measurement of gravity were performed “in the air”. For the vertical gradient determination the measurements at two elevations with the difference of precisely ( $\pm 0.005$  m) 1 m have been utilized using a tripod (Fig. 3). The measurement sequence (B-A-B-A) at each station required 20 to 30 minutes. The letter A stands for the lower position of the instrument (on the floor), the upper position of the gravimeter on the tripod (1 m above the floor) is denoted by B. The data were drift-corrected in the usual manner. The value of the measured vertical gradient, i.e.  $-0.281 \pm 0.0036$  mGal/m, was used later during data processing. Most important corrections in the frame of final Bouguer anomaly evaluation (discussed in the following section) were computed using the downward continuation of gravity from the wooden steps to the floor on these seven highest stations in the apse, utilizing the measured vertical gradient value.

#### 4. Data processing

In the interpretation of microgravity surveys the relative variations in the local gravity field are important. Therefore, the data do not need to be corrected to the absolute gravity. The latitude correction could be neglected due to the small dimensions of the survey area. The most important steps of the incomplete Bouguer anomaly evaluation were the the free air and the planar Bouguer slab corrections (using an estimated correction density of  $2.0 \text{ g/cm}^3$ ). Adapting these corrections as close as possible to the real situation, we have tested three different approaches, which will be described in more detail below. When the survey is carried inside the buildings, nearby man-made structures decrease the measured value of gravity on the closest stations due to their gravitational attraction. Gravitational effects of buildings can reach several  $\mu\text{Gal}$  up to hundreds of  $\mu\text{Gal}$ . These effects and undulating topography have to be properly established, as they can be greater than the amplitude of the expected anomalies. The various components of the buildings can be approximated by a summation of polygonal



Fig. 3. Vertical gravity gradient measurement; the CG-5 gravimeter is placed on a tripod in the upper position (1 m elevation difference).

prisms with vertical edges (*Blízkovský, 1979; Debeglia and Dupont, 2002*). For the description of the whole church 46 polygonal prisms were used. To each component elevations for the top and base, a thickness for the walls and an estimated mean density contrast of  $1.75 \text{ g/cm}^3$  were assigned. The walls, pillars and altar are located above the average ground height (362 m), and present a positive density contrast. The calculated building effect is negative, decreasing strongly towards the apse, fundamentally influencing the shape of the resultant anomaly (Figs. 5a and 5b). The minimum amplitude of the correction is relatively low, i.e.  $-120 \mu \text{ Gal}$  (Fig. 5b).

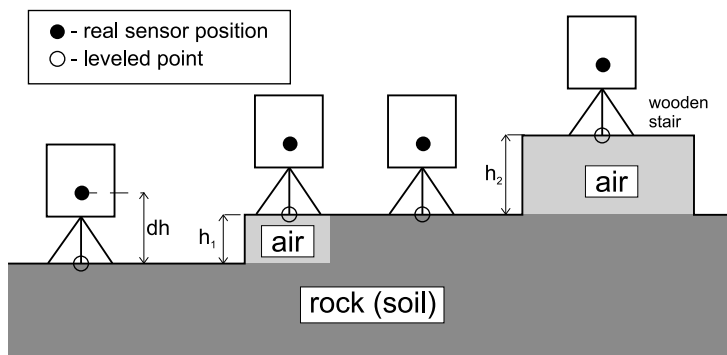


Fig. 4. Scheme, showing the typical positions of the measurement points and the real situation of the sensor position;

$dh$  – vertical displacement of the sensor from the floor (approx. 26 cm),

$h_1$  – average elevation difference between the apse and the nave (approx. 19 cm),

$h_2$  – average elevation difference of the highest wooden stairs in the apse (approx. 33 cm).

A terrain correction was not required because the area of the church close surroundings is sufficiently flat and the elevation differences among measuring points are relatively small. The final Bouguer anomaly map (Fig. 5c) shows a dominating trend in W-E direction, together with the significant negative anomaly in the upper part of the area. The regional trend was approximated by a simple planar surface and removed from the data. Fig. 8 shows the residual Bouguer anomaly map with a range of  $\pm 40 \mu\text{Gal}$ .

As we have mentioned above, the corrections in the frame of the final Bouguer anomaly evaluation have been calculated using three different approaches in this case-study:

1. The first one, denoted as “Standard”, ignores the fact that the real position of the sensor inside of the instrument is in some vertical displacement above the ground (J. Mikuška, personal communication) and that some of the measuring points have been localized at wooden stairs (disregarding the fact that there is an empty space inside the stair between the measurement point position and the floor). The free air, planar Bouguer slab and building effect corrections have been evaluated for the leveled elevations of the measurement points (as it is common in applied gravimetry).

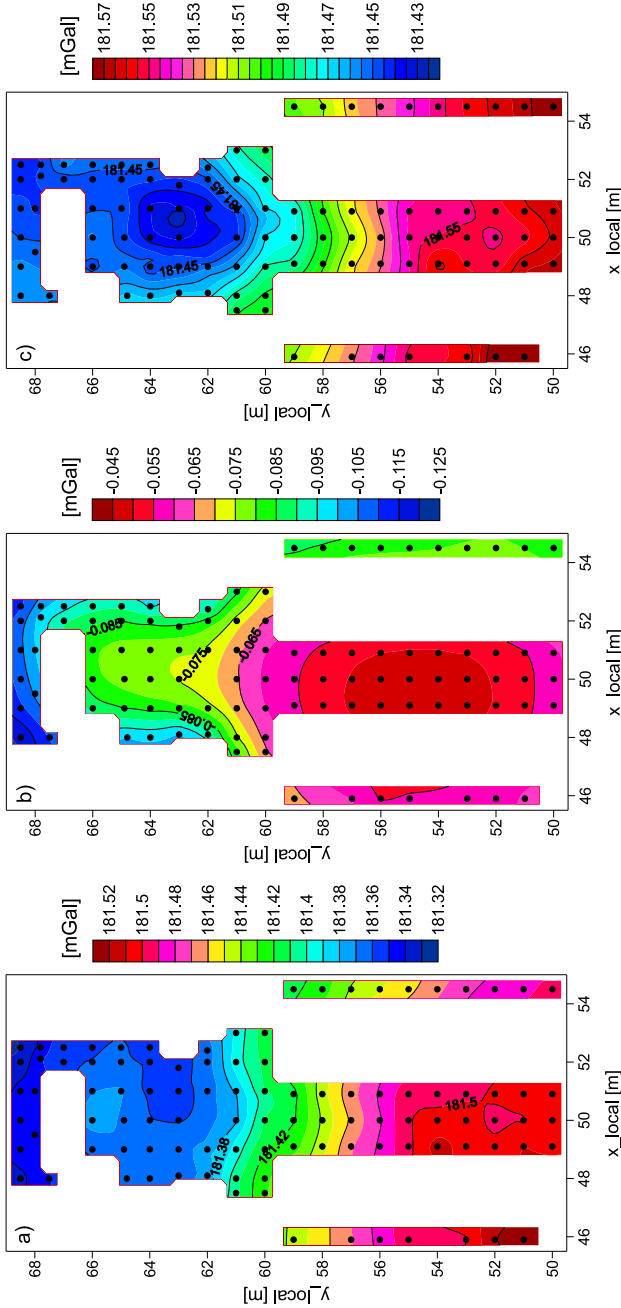


Fig. 5. The sequence of steps used in the final Bouguer anomaly map creation: a) incomplete Bouguer anomalies in [mGal] for the correction density  $2.0 \text{ g/cm}^3$ ; b) modelled effect of buildings walls in [mGal] for density of  $1.75 \text{ g/cm}^3$ ; c) final Bouguer anomalies (subtracted correction for building effect) in [mGal].

2. Using the second one, denoted as “Sensor position”, we have tried to resolve the problems depicted with the first approach. The free air and building effect corrections have been evaluated in the real position of the sensor in the instrument. This vertical displacement, denoted as  $dh$  (Fig. 4), was approximately 26 cm (17 cm was the average height of the tripod and 8.9 cm is the vertical distance of the sensor position from the bottom edge of the instrument – CG-5 Scintrex Autograv System Operation manual, see p. 1–8) and it was added to the leveled elevation of each measurement point. The planar Bouguer slab correction was evaluated directly for the leveled elevation without any adjustment. A special situation occurred in the case of eighteen points, which have been positioned on a wooden stairs in the apse (Fig. 2 – marked by triangles). In this case, the planar Bouguer slab correction was evaluated for the leveled elevation minus the elevation difference of the stairs ( $h_1$  and  $h_2$  in Fig. 4) – with this processing step we wanted to accept the fact that the stairs have been empty and the rock (soil) masses, described by the Bouguer slab, are lower (at the solid floor of the apse).
3. The third one (“Downward continued”) is a relatively new experiment. It is based on a downward continuation of the measured gravity on seven (highest) points to the level of the surrounding points in the apse, followed by the same final Bouguer anomaly evaluation as in the second approach. The main reason for this experiment was the fact that some of the interpretation tools require the data set on an approx. identical elevation level (e.g. transformations such as the higher derivatives evaluation, analytical continuation). The height difference used for the downward continuation of the measured gravity values was equal to the average height of the highest wooden stair ( $h_2$  in Fig. 4, approx. equal to 33 cm), using the real measured value of the vertical gravity gradient (0.281 mGal/m). This value is 8.9% lower than the normal value of 0.3086 mGal/m.

The comparison of these three approaches for seven points located on wooden steps is summarized in Table 1 and the character of final Bouguer anomaly maps displayed in Figs. 6 and 7. The first column in Table 1 contains the point numbers, while the others compare the values of incomplete Bouguer

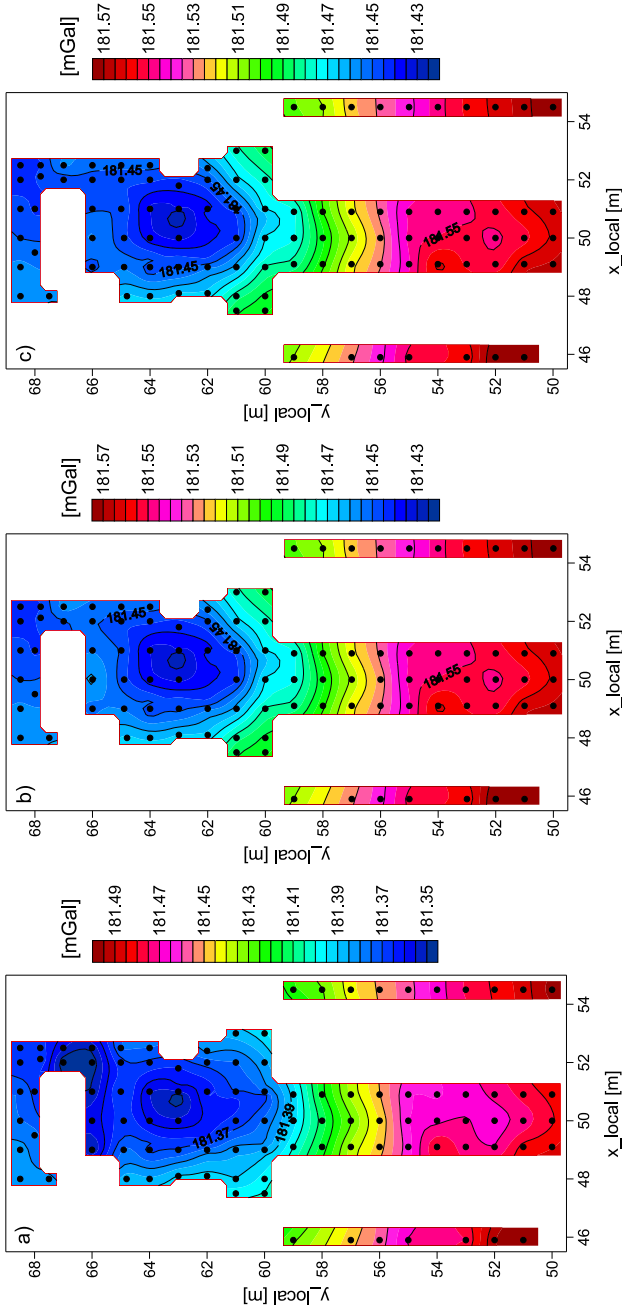


Fig. 6. The final Bouguer anomaly maps obtained by means of: a) “Standard” approach [mGal]; b) “Sensor position” approach [mGal]; c) “Downward continued” approach [mGal].

anomalies, corrections for building effect and final Bouguer anomalies for the three different approaches realized. As it can be seen in Figs. 6 and 7, there are relatively great differences between the final Bouguer anomalies obtained by means of the “Standard” approach and the other two ones. The most important feature in the “Standard” approach map is the existence of a small false negative anomaly in the area of the highest wooden step in the apse ( $y = 66\text{--}67$  m,  $x = 50\text{--}52$  m) (Fig. 6a). The absolute value of the false anomaly amplitude gets up to  $30 \mu\text{Gal}$  (Figs. 7a and 7c), which is very high and it was caused by the incorrect removal of the planar Bouguer slab effect in a space, which was filled by air and not subsequently corrected by an appropriate terrain correction. This false anomaly disappears in maps, obtained by means of the “Sensor position” and “Downward continued” approaches (Figs. 6b and 6c). The difference between the latter two maps is very small (its absolute value is reaching only  $5 \mu\text{Gal}$ , Fig. 7b) – very close to the root-mean-square error of the data acquisition process. For the further interpretation process, we selected the final Bouguer anomaly field, obtained by means of the “Downward continued” approach, because we think it describes the real situation the best.

## 5. Interpretation of anomalous feature

For the qualitative and quantitative interpretation process the residual Bouguer anomaly map was used, obtained from the “Downward continued” final Bouguer anomaly map by means of a subtraction of a simple planar surface (linear trend). This map was created by the grid subtraction in the Surfer software. For further interpretation, the area bounded by a rectangle (Fig. 8) was used. The main feature, clearly noticeable in the final residual Bouguer anomaly map, is a negative anomaly located in the apse, with amplitude exceeding  $-30$  up to  $-40 \mu\text{Gal}$ . One of the possible interpretations of this negative anomaly is the existence of an underground crypt.

In order to estimate the dimensions and depth of the anomaly source, two methods were employed. The crypt was modelled using density modelling as two 3D polygonal prisms (Fig. 9). In Fig. 9a, the upper view on modelled air-filled crypt is displayed. Fig. 9b shows the cross-section along the E-W

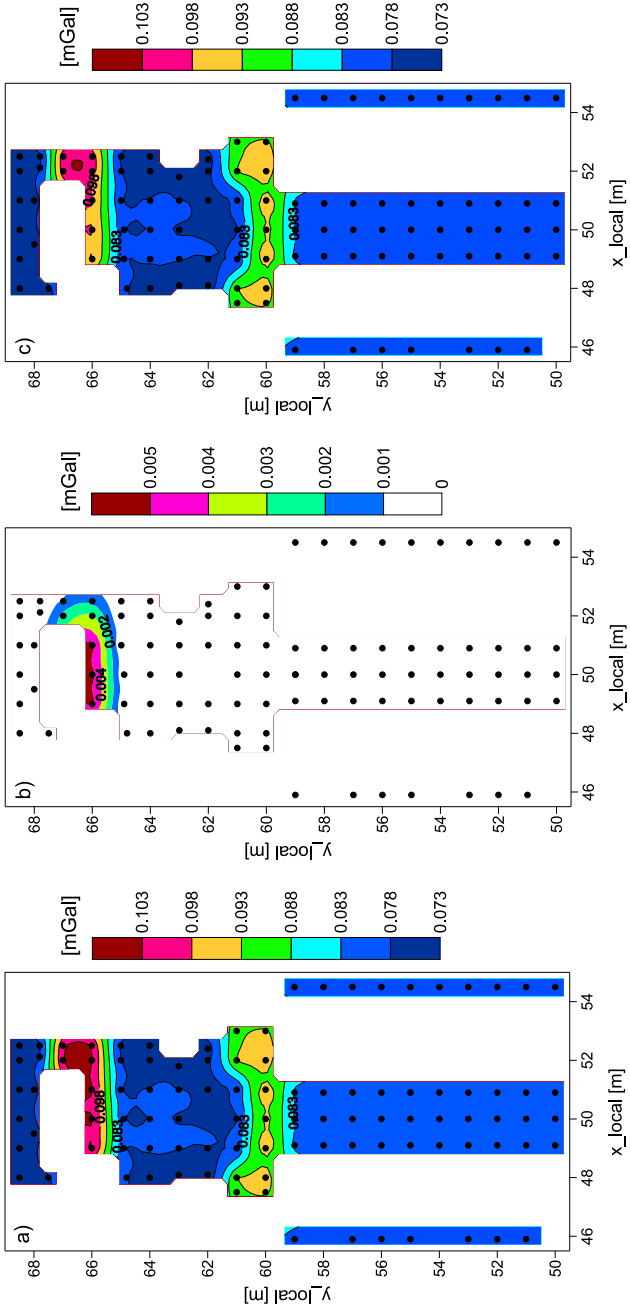


Fig. 7. Differences between the final Bouguer anomaly maps: a) “Sensor position” minus “Standard” [mGal]; b) “Sensor position” minus “Downward continued” [mGal]; c) “Downward continued” minus “Standard” [mGal].

Table 1. The comparison of three approaches of the final Bouguer anomalies evaluation

Point number	Incomplete Bouguer anomalies [mGal]			Corrections for building effect [mGal]			Final Bouguer anomalies [mGal]		
	<i>Standard</i>	<i>Sensor position</i>	<i>Downward continued</i>	<i>Standard</i>	<i>Sensor position</i>	<i>Downward continued</i>	<i>Standard</i>	<i>Sensor position</i>	<i>Downward continued</i>
4966	181.262	181.369	181.361	-0.087	-0.084	-0.088	181.349	181.453	181.449
5066	181.276	181.384	181.376	-0.081	-0.078	-0.081	181.357	181.462	181.457
5166	181.270	181.378	181.369	-0.080	-0.077	-0.081	181.350	181.455	181.450
5266	181.261	181.369	181.360	-0.085	-0.081	-0.086	181.346	181.450	181.446
5267	181.256	181.364	181.355	-0.089	-0.085	-0.091	181.345	181.449	181.446
5366	181.260	181.368	181.359	-0.091	-0.086	-0.092	181.351	181.454	181.451
5367	181.260	181.368	181.359	-0.096	-0.090	-0.097	181.356	181.458	181.456

Profile 1. The depth and shape of the modelled crypt were varied, until an acceptable fit between the observed (red line) and calculated (blue line) fields was achieved. The discrepancy between the observed and calculated fields at the end of Profile 1 in Fig. 9b can be explained by an inadequate determination of corrections for building effect or by a deformation of the residual anomaly field (by removing the simple planar surface during the residual field separation). Fig. 9b shows that the crypt could be situated approx. 1 m under the floor in the apse.

The depth of causative body was estimated also by the 3D Euler deconvolution algorithm. Euler deconvolution is a widely-used method for locating the sources of potential fields based on both their amplitudes and gradients and an estimate on the probable geometry of the causative body (Thompson, 1982; Reid et al., 1990). The structural index (defining the type of searched anomalous structure) was set to 2, detecting the centre of a body with a spherical shape. The position of the solution cluster is partly defocused from the centre of the anomaly (Fig. 9a), which can be explained by small deformations of the anomalous field (existence of measurement errors and imperfect evaluation of the building effect corrections) or by the deficiency of the method itself. Average depths of the solution cluster fit into the depth extent of the anomalous structure, obtained by means of 3D density modelling (they are slightly shifted to the top).

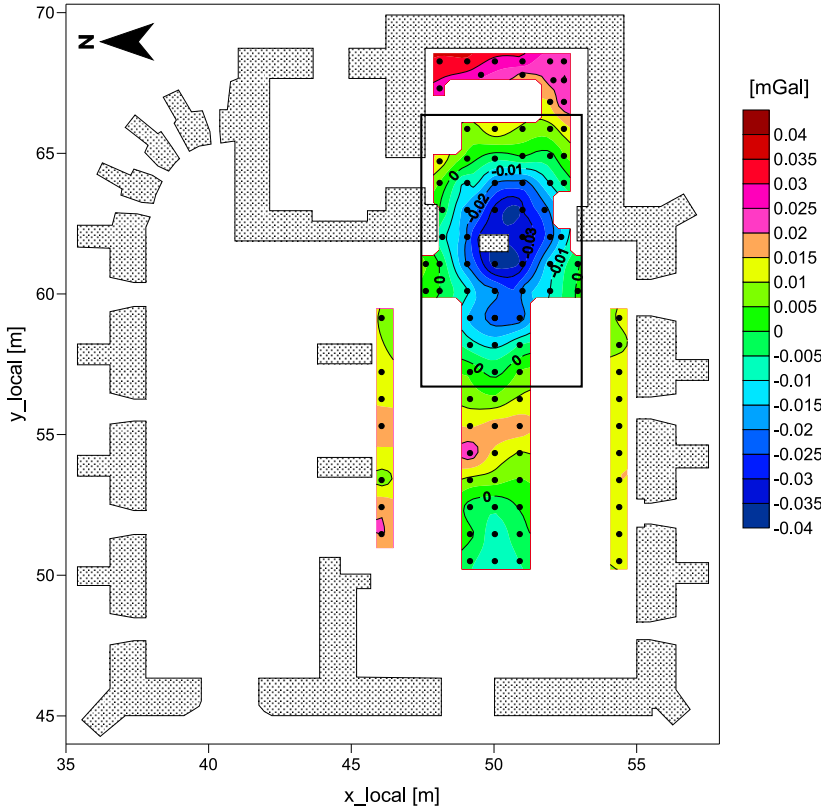


Fig. 8. The residual Bouguer anomaly map of the survey area based on the “Downward continued” approach (after removing a simple planar surface describing the regional component of the Bouguer anomaly field) in [mGal]. The highlighted area was interpolated with a step of 0.5 m and used for further interpretation of the acquired negative anomaly.

## 6. Conclusions

The microgravity technique is shown to be a very effective and non-destructive tool for the detection of man-made cavities in old historic buildings. This paper has presented an example of microgravity data collected in the St. Nicolas church in Pukanec in order to map out the possible subsurface void features. With a careful field acquisition, the Scintrex CG-5 gravimeter was shown to be adequate for shallow subsurface target location in archaeology. Considerable emphasis was placed to the data processing, especially to

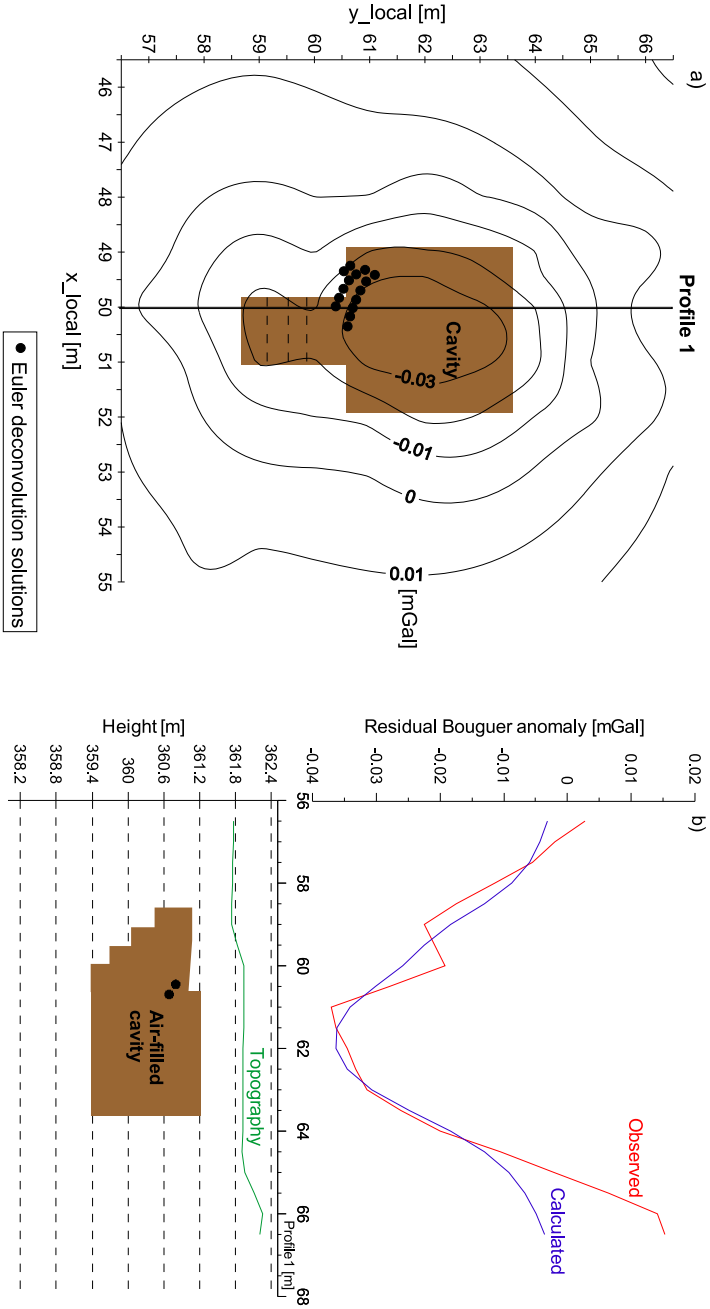


Fig. 9. Three-dimensional model of sub-surface interpretation: a) upper view of modelled air-filled cavity and observed field; b) a view of the possible location and shape of the crypt – results along E-W Profile 1: observed field (red line), calculated field (blue line). Filled circles denote positions of the 3D Euler deconvolution depth estimates.

the evaluation of the building effect, which could produce false negative signals and deform the interpreted Bouguer anomaly field. Three approaches of final Bouguer anomalies evaluation were compared. The first was the classical one based on the free air and planar Bouguer correction (ignoring the fact that the real position of the instrument sensor is not in the point, which is leveled and that some of the measurement points have been positioned on wooden steps – like they would be ‘in free air’). The second one has accepted this fact and evaluated the corresponding corrections in the real position of the sensor. The third one was based on a downward continuation of the measured gravity for seven highest points (utilizing the real measured vertical gravity gradient) to the level of the surrounding points on the solid floor, followed by the same steps as in the second approach. The most important feature in the “Standard” approach map is the presence of a small false negative anomaly in the area of the highest wooden stair (with the absolute value of max.  $30 \mu\text{Gal}$ ). This false anomaly disappears in maps obtained by means of the “Sensor position” and “Downward continued” approaches. The influence of the downward continuation of gravity to the same height level by the real vertical gravity gradient on the amplitude and shape of the final Bouguer anomaly map is very small and both maps are qualitatively on the same level. This is caused by the fact that the height differences among the different stations are small (below 0.5 m).

Significant negative anomaly was obtained from the final residual Bouguer anomaly map. Euler deconvolution provided approx. positions and depths to the anomaly source. The shape and depth of possible crypt were estimated using 3D density modelling. The results show that the crypt could be situated approx. 1 m under the floor in the apse.

Finally, we can claim, based on the qualitative (shape and amplitude of the anomaly) and quantitative (3D Euler deconvolution and 3D density modelling) interpretations, that the presence of medieval crypt in the apse of the church is highly probable. However, it must be accompanied by the GPR measurements and subsequent opening or video inspection.

***Acknowledgments.*** This work was performed with the support of the VEGA Grant Agency under projects No. 2/0107/09 and 1/0461/09, as well as the DFG Mercator INST 5659/1-1. The authors express their thanks for valuable discussions and help with improving the manuscript to Pavol Zahorec.

## References

- Bishop I., Styles P., Emsley S. J., Ferguson N. S., 1997: The detection of cavities using the microgravity technique: case histories from mining and karstic environments. *Modern Geophysics in Engineering Geology*, Geological Society, Engineering Geology Special Publication, **12**, 153–166.
- Blížkovský M., 1979: Processing and applications in microgravity surveys. *Geophysical Prospecting*, **27**, 4, 848–861.
- Butler D. K., 1984: Microgravimetric and gravity gradient techniques for detection of subsurface cavities. *Geophysics*, **49**, 7, 1084–1096.
- CG-5 Scintrex Autograv System Operation Manual. Scintrex Ltd. Toronto, Canada, Nr. 867700 Rev. 4, p. 308 (April 2009).
- Cuss R. J., Styles P., 1999: The application of microgravity in industrial archaeology: an example from the Williamson tunnels, Edge Hill, Liverpool. *Geoarchaeology: exploration, environments, resources*. Geological Society, London, Special Publications, **165**, 41–59.
- Debeglia N., Dupont F., 2002: Some critical factors for engineering and environmental microgravity investigations. *Journal of Applied Geophysics*, **50**, 4, 435–454.
- Fajkiewicz Z., 1976: Gravity vertical gradient measurements for the detection of small geologic and anthropogenic forms. *Geophysics*, **41**, 5, 1016–1030.
- Lakshmanan J., Montlucon J., 1987: Microgravity probes the Great Pyramid. *Geophysics: The Leading Edge of Exploration*, **6**, 1, 10–17.
- Owen T. E., 1983: Detection and mapping of tunnels and caves. In: Fitch A. A., (Ed.), *Development in Geophysical Exploration methods*, **5**, 161258, Wiley, 209–221.
- Pašteka R., Zahorec P., 2000: Interpretation of microgravimetric anomalies in the region of the former church of St. Catherine, Dechtice. *Contr. Geophys. Geod.*, **30**, 4, 373–387.
- Pašteka R., Terray M., Hajach M., Pašiaková M., 2007: Microgravity measurements and GPR technique in the search for medieval crypts: a case study from the St. Nicholas church in Trnava, SW Slovakia. *Proceedings of the Archaeological Prospection 7<sup>th</sup> conference, Nitra, Štúdijné zvesti*, **41**, 222–224.
- Reid A. B., Allsop J. M., Garner H., Millett A. J., Somerton I. W., 1990: Magnetic interpretation in three dimensions using Euler deconvolution. *Geophysics*, **55**, 1, 80–91.
- Terray M., Pašteka R., 2007: Využitie geofyzikálnych metód merania pri vyhľadávaní podzemných objektov na príklade Kostola sv. Mikuláša v Trnave. *Pamiatky Trnavy a Trnavského kraja*, **10**, 17–24.
- Thompson D. T., 1982: EULDPH: A new technique for making computer-assisted depth estimates from magnetic field data. *Geophysics*, **47**, 1, 31–37.